Study on the Carrier Lifetime of RGB Mini-Light-Emitting Diodes Based on Phase-Sensitive Detection

Chen-Ming Zhong, *Graduate Student Member*, *IEEE*, Jing-Yu Deng, Xi Zheng, Chang-Dong Tong, Guo-Bao Zhao, Guo-Long Chen, Hui-Hui Meng, Li-Hong Zhu, Yi-Jun Lu, Zhong Chen, and Wei-Jie Guo, *Member*, *IEEE*

***Abstract*—A differential carrier lifetime (DLT) measurement method with a measurement current as low as 0.1 mA, high noise immunity, and low measurement error has been proposed for the first time for electroluminescent LEDs, which can also obtain the junction capacitance and differential resistance of LEDs. The method is based on the rate equation and phase-sensitive detection technology. The relationship between the DLT of red, green, and blue mini-LEDs and the injected current density was investigated with the proposed method. The DLT of the same LED decreases as the injected current density increases. The DLT of green mini-LEDs drops faster than that of blue mini-LEDs as the injected current density increases.**

***Index Terms*—Carrier lifetime, differential resistance, light-emitting diodes, lock-in amplifier.**

I. Introduction

HIGH-SPEED light-emitting diodes (LEDs) have recently sparked interest in future light-fidelity (Li-Fi) networks for visible light communication (VLC) [1], [2] and visible light localization [3], [4]. VLC systems with data rates of more than 10 Gb/s have been demonstrated when combined with multiplexing techniques and advanced modulation schemes [5]. In general, a higher bandwidth is obtained by lowering both the LED transport-related time constants and the carrier lifetime. Methods to characterize the carrier lifetime of LEDs are one of the current hot topics in semiconductor research. Time-resolved photoluminescence (TRPL) is one of the methods to characterize the carrier lifetime, but the method focuses more on carrier lifetime measurement under photoluminescence conditions. The TRPL results for LEDs are influenced by the laser focal region and the structure layer and do not provide sufficient guidance on the electroluminescent LED carrier lifetime because TRPL ignores carrier transport effects through the LED structure [6]. Haggar *et al*. proposed a time-resolved electroluminescence (TREL) method to determine the carrier lifetime of a semipolar green light-emitting diode by fitting the falling edge of the received optical signal [6]. The test results of the method are influenced by the signal-to-noise ratio of the received optical signal and the type of fitted polynomial. Rashidi *et al*. optimized the LED small-signal equivalent model and used the LED impedance to fit the circuit parameters in the proposed model to determine the differential carrier lifetime of the LED [7]. There are also methods of fitting the LED impedance based on the LED equivalent model to obtain the differential resistance and capacitance parameters of the LED and then calculating the differential carrier lifetime [8], [9]. Because the carrier lifetime of a LED is closely related to the bandwidth of VLC, some researchers have calculated the carrier lifetime by testing the bandwidth of the LED [10], [11]. Richard *et al*. used a network analyzer and a silicon photodetector to measure the -3 dB bandwidth of a LED to calculate the differential carrier lifetime [11]. Determining the bandwidth of LEDs by measuring their carrier lifetime is an effective method, but the LED bandwidth in VLC systems is affected by the carrier lifetime, drive circuits, modulation mode, etc. Therefore, the error in using the LED bandwidth to calculate the differential carrier lifetime may be relatively large. Reklaitis *et al*. used a 405 nm laser to induce photoluminescence of a LED and then tested the phase difference between the transmitted and received optical signals to determine the LED differential carrier lifetime [12]. A lock-in amplifier based on phase-sensitive detection is used for phase difference measurements to improve the accuracy of carrier lifetime tests. However, this method is similar to TRPL in that it employs the principle of LED photoluminescence, in which the carrier lifetime of the LED is limited by the laser focal position and power. Increasing the optical power of the laser increases the photogenerated current of the LED, but it also tends to burn out the LED. Meng *et al*. used a signal amplifier and a dual-channel oscilloscope to build a system for testing the differential carrier lifetime of LEDs [13]. The LEDs were driven with a small-amplitude AC signal at a DC bias, and the optical signal was received by a photodetector, with the differential carrier lifetime determined by testing the phase difference between the transmitted and received signals. The system employs discrete components containing parasitic capacitance and inductance, such as preamplifiers and load

This work was supported in part by the National Natural Science Foundation of China under Grant 62275227, 62274138, 11904302, in part by the Science and Technology Project of Fujian Province under Grant 2023H4028, in part by the Key Research and Industrialization Projects of Technological Innovation of Fujian Province under Grant 2022G043, in part by the Shenzhen Science and Technology Program under Grant JCYJ20220530143407017. (Corresponding author: Zhong Chen; Wei-Jie Guo.)

C. M. Zhong, J. Y. Deng, X. Zheng, C. D. Tong, G. B. Zhao, G. L. Chen, L. H. Zhu, Y. J. Lu, Z. Chen, and W. J. Guo are with the National Innovation Platform for the Fusion of Industry and Education in Integrated Circuits, Department of Electronic Science, School of Electronic Science and Engineering, Xiamen University, Xiamen 361005, China, and also with Shenzhen Research Institute of Xiamen University, Shenzhen 518057, China (e-mail: chenz@xmu.edu.cn; wjguo@xmu.edu.cn).

H. H. Meng is with Guangzhou Sine Scientific Instrument Co., Ltd., Guangzhou 510399, China.

resistances, and the components are not phase-calibrated and have limited capabilities for weak optical signal reception and noise immunity.

Previous measurements of the differential carrier lifetimes have been achieved by three methods: TRPL, fitting the falling edge of the received optical signal, or fitting the equivalent circuit parameters by the impedance of the LED. However, TRPL excites the LED with a laser, and the measurement results are influenced by the laser focusing area and the structural layer on which it is focused. It also ignores carrier transport effects through the LED structure, which cannot provide sufficient guidance for the carrier lifetime of electroluminescent LEDs. Different fitting functions or RLC-circuit models of the LED may produce different results, and it is difficult to guarantee the accuracy of the results when the optical signal is weak. Determining the carrier lifetime of LEDs by testing the bandwidth of VLC systems introduces large errors due to the use of signal amplification, transmit-receive equalizers, different modulation methods, and impedance matching components in VLC systems to increase the bandwidth. The measurement system employs discrete devices with more parasitic parameters, especially parasitic capacitance and inductance, which can cause undesirable phase lead-lag effects (In the time domain, when an AC signal is transmitted through cables, signal amplifiers, etc., it arrives earlier than the reference signal at a certain point in time, which is called phase lead and, conversely, phase lag) when the phase difference is used to determine the differential carrier lifetime and therefore have a great impact on the accuracy of the test results. The operating current range of the LED plays an important role in the modulation depth of the VLC system [14]. The modulation depth can be defined as (peak current-bias current)/bias current. The lower the bias current is, the higher the modulation depth, and the easier the visible light signal can be detected by the photodetector, which can reduce the transmitting power required by the optical transmitter. For higher-order modulation methods, such as M-level pulse amplitude modulation, the LED operating scenarios include a low current case, which facilitates optical signal processing and improves the bandwidth [15]. It is interesting to explore a method that can support measurement of the carrier lifetime in the case of low current driving of LEDs and for which the test system uses fewer discrete devices.

In this paper, we propose a differential carrier lifetime measurement method for electroluminescent LEDs for the first time that has high noise immunity, low measurement error, and advantageously supports LED operation in low-current scenarios. The proposed method offers a way to study the differential carrier lifetime, junction capacitance, and differential resistance of LEDs.

II. Measurement System

The measurement system consists of a power source (Keysight B2911, Keysight Inc.), a digit graphical sampling multimeter (Keithley DMM7510, Keithley Inc.), a temperature controller (TECSource 5305, Arroyo Instruments, LLC), a DSP lock-in amplifier (Model OE2031, Guangzhou Sine Scientific Instrument Co., Ltd.), a spectrometer (QE65Pro, Ocean Insight Inc.), an integrating sphere (FOIS-1, Ocean Insight Inc.), and a PIN photodetector (S5973, Hamamatsu Photonics Co., Ltd), as shown in Fig. 1. The lock-in amplifier (LIA) generates a sinusoidal AC voltage signal (amplitude: 50 mV) using an internal reference clock, receives an external DC input, sums the AC and DC signals, and drives the LED. The light emitted from the LED passes through the integrating sphere and an optical fiber and is then received by the spectrometer and the PIN photodetector, respectively. The photodetector converts the optical signal into an electrical signal and sends it to the LIA, while the spectrometer acquires the LED spectra at the same time. The optical fiber plays a light-splitting role in the optical path. The response frequency of the photodetector should be much larger than the detection frequency, at least 2 times the detection frequency to satisfy Nyquist's sampling theorem. The photodetector bandwidth for the proposed measurement method is 1 GHz, which satisfies the test requirements. Considering the input noise and operating frequency of the system, a time constant of 1 ms is used uniformly for the DSP lock-in amplifier during testing. The experimental procedure was as follows:

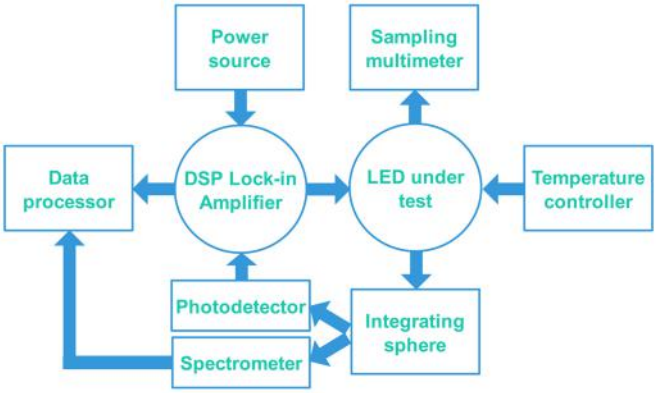

Fig. 1. Schematic diagram of the measurement setup.

1) The temperature controller maintains the LED at the desired temperature. Pretest calibration of the system and components, including phase calibration of the transmit and receive signal cables, is performed. The cable calibration for this work is completed by the DSP Lock-in amplifier. The cable to be calibrated is connected between the input and output of the DSP Lock-in amplifier to measure the phase delay at different operating frequencies.

2) The differential carrier lifetime of the LEDs with different injected currents and AC frequencies are measured by the LIA.

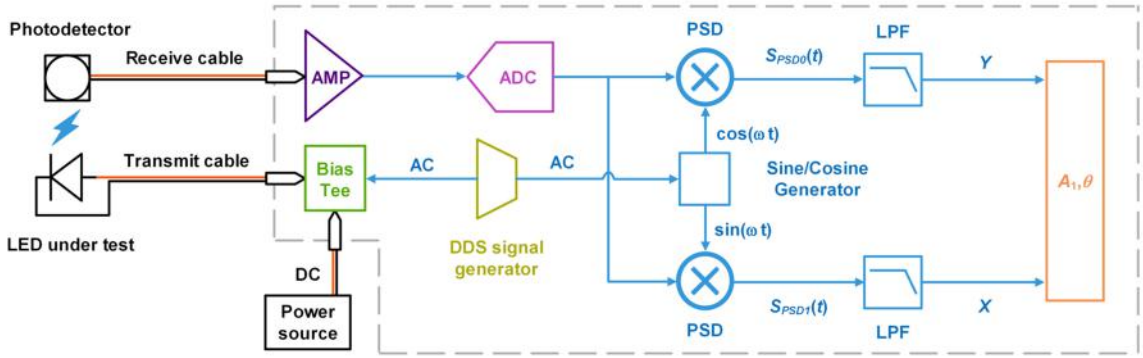

Fig. 2. Block diagram of the measurement system.

3) The spectra of LEDs are acquired for different samples under the same conditions.

Commercial red, green, and blue mini-LEDs (RGB mini-LEDs, Xiamen Changelight Co., Ltd.)—red (201 μm × 106 μm), green (202 μm × 98 μm), and blue (202 μm × 94 μm)—were tested in this work.

III. System Principle

In a LED, electrons and holes are injected and recombine in pairs. Assuming that N denotes the number of electrons, the rate of increase in the number of electrons in the active region is given by [16]:

$$\frac{dN}{dt}=\frac{I}{q}-\frac{N}{\tau_c}, \tag{1}$$

where q denotes the electronic charge, I denotes the injected current, and τ_c denotes the recombination time constant. The rate of electron injection into the active region is given by the first term on the right side of (1), and the rate of electron-hole recombination, including radiative and nonradiative recombination, is given by the last term. The current injected into the LED is a combination of the DC bias current (I_b) and sinusoidal modulation current ($I_m e^{j\omega_m t}$), which can be expressed as follows:

$$I=I_b+I_m e^{j\omega_m t}, \tag{2}$$

where ω_m represents the angular frequency of the sinusoidal modulation current. Substituting (2) into (1) and solving for the steady-state carrier number gives:

$$N(t)=N_b+N_m e^{j\omega_m t}, \tag{3}$$

where $N_b=I_b\tau_c/q$, and

$$\frac{qN_m}{\tau_c}=\frac{I_m}{1+j\omega_m\tau_c}, \tag{4}$$

where N_b denotes the carrier number due to the DC bias current and N_m denotes the carrier number due to the sinusoidal modulation current. According to (4), the amplitude decreases with the modulation frequency. It is clear that the left-hand side of (4) is the current directly responsible for carrier recombination. This current can be approximated as the current generated by an AC photon, whose amplitude is expressed as I_p [16]. Thus, (4) represents the LED frequency response relationship between the photon current I_p and the sinusoidal current I_m and can be rewritten as follows:

$$\frac{I_m e^{j\omega_m t}}{I_p e^{j(\omega_m t-\phi)}}=1+j\omega_m\tau_c. \tag{5}$$

$I_m e^{j\omega_m t}$ and $I_p e^{j(\omega_m t-\phi)}$ can be approximated as same-frequency but different-phase signals; according to (5), assuming that the phase difference ϕ can be measured, τ_c is then given by:

$$\tau_c=\frac{\tan(\phi)}{\omega_m}. \tag{6}$$

The frequency response is known to be the same as that of a parallel RC circuit, and the RC time constant is approximately equal to τ_c [17]. The recombination time constant τ_c is also denoted as the differential carrier lifetime because it is based on an RC circuit [18], [19]. The $I_p e^{j(\omega_m t-\phi)}$ signal is collected by a photodetector and fed into a lock-in amplifier to obtain the phase of $I_p e^{j(\omega_m t-\phi)}$, and the phase difference with $I_m e^{j\omega_m t}$ is extracted to determine τ_c in the method proposed in this paper.

The core principle of the LIA operation is phase-sensitive detection (PSD), which involves multiplying the input signal by the reference signal and then filtering it with a low-pass filter (LPF) [20]. PSD is widely used because of its advantages in extracting the phase and frequency of signals as well as its anti-interference capability. Carrier lifetime measurements based on PSD applied to photoluminescence have been reported previously [21], [22]. The block diagram of the measurement system proposed in this paper is shown in Fig. 2. The LIA typically contains two PSDs and two LPFs. The input signal to be measured, $S(t)$, can be defined as follows:

$$S(t)=A_1\sin(\omega t+\varphi)+B(t), \tag{7}$$

where A_1, φ and $B(t)$ represent the amplitude, phase, and total

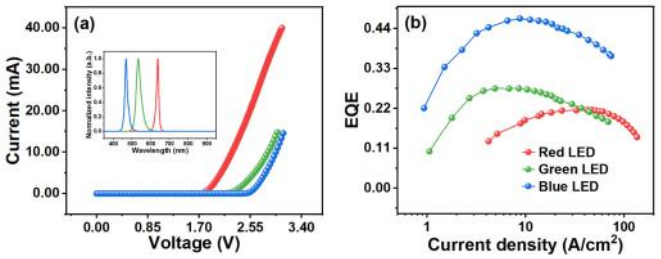

Fig. 3. (a) *I-V* curve (inset: normalized spectrum of RGB mini-LEDs at a drive current of 2.00 mA), and (b) EQE curve of RGB mini-LEDs at a controlled temperature of 300 *K*.

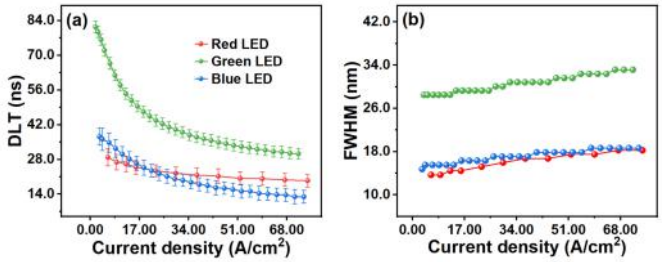

Fig. 4. (a) DLT curve with varied injected current density, and (b) FWHM of the samples at a controlled temperature of 300 *K*.

noise, respectively. ω (ω=2 πf) represents the angular frequency of the input signal. The internal direct digital synthesis (DDS) signal generator of the LIA produces AC signals, one of which is fed into a bias tee, and the other is used as a signal to generate two subreference signals ($S_{Ref0}(t)$ and $S_{Ref1}(t)$) via a sine/cosine generator. The two subreference signals can be defined as:

$$\begin{cases} S_{Ref\,0}(t) = A_R \cos(\omega t + \delta) \\ S_{Ref\,1}(t) = A_R \sin(\omega t + \delta) \end{cases}, \tag{8}$$

where A_R and δ represent the amplitude and phase of the input reference signal, respectively. The bias tee completes the superposition of the AC signal with the external input DC signal and then drives the LED. The photodetector receives the LED light signal and converts the light signal to an electrical signal, which is then fed into the LIA. The input signal is sent to the PSD after passing through the LIA internal amplifier (AMP) and analog-to-digital converter (ADC). The input signal to be measured and two subreference signals are simultaneously fed into the PSD module for multiplication. The outputs of the two PSDs are as follows:

$$\begin{aligned} S_{PSD0}(t) &= \frac{1}{2} A_R A_1 \sin(\varphi - \delta) \\ &\quad - \frac{1}{2} A_R A_1 \sin(2\omega t + \varphi + \delta) + B(t) A_R \cos(\omega t + \delta), \end{aligned} \tag{9}$$

$$\begin{aligned} S_{PSD1}(t) &= \frac{1}{2} A_R A_1 \cos(\varphi - \delta) \\ &\quad - \frac{1}{2} A_R A_1 \cos(2\omega t + \varphi + \delta) + B(t) A_R \sin(\omega t + \delta). \end{aligned} \tag{10}$$

After using the LPF to filter out the AC signal and noise, the final DC components are X and Y, as follows:

$$\begin{cases} X = \frac{1}{2} A_1 A_R \cos(\varphi - \delta) \\ Y = \frac{1}{2} A_1 A_R \sin(\varphi - \delta) \end{cases}. \tag{11}$$

By calculating the square roots of X and Y, the unknown quantities can be eliminated, and the amplitude A_1 of the signal to be measured and the phase difference θ between the signal to be measured and the reference signal can be obtained as follows:

$$\begin{cases} A_1 = \frac{2\sqrt{X^2 + Y^2}}{A_R} \\ \theta = \varphi - \delta = \arctan(Y / X) \end{cases}. \tag{12}$$

Assuming that the transmit and receive signal cables introduce a phase delay of $\triangle\theta$ for the signal to be measured, the actual phase difference is θ-$\triangle\theta$. The photodetector does not have a discrete signal amplifier installed, and the LIA is responsible for amplifying the received light signal to minimize the parasitic parameters brought by the introduction of discrete devices.

Combining (6) and (12), the differential carrier lifetime (DLT) of the LED can be expressed as:

$$\mathrm{DLT} = \frac{\tan(\arctan(Y / X) - \Delta\theta)}{2\pi f}. \tag{13}$$

The frequency response of LEDs represents the relationship between the modulation frequency and output power. The power transfer function of a LED device can be expressed as [23]:

$$P(f) = \frac{1}{\sqrt{1 + (2\pi f \tau)^2}}, \tag{14}$$

where $P(f)$ denotes the frequency response function, τ denotes the time constant, and f denotes the modulation frequency. When the LED is driven at a constant current, τ remains nearly constant. When f is increased, $P(f)$ decreases, and the AC amplitude of the LED light signal is weakened, causing more error in light signal detection at the receiving terminal. For higher f, the signal is too weak to be accurately measured, whereas for much lower f, the relative error becomes significant due to the small phase difference [13]. Therefore, the DLT was measured using (13) at a controlled temperature of 300 *K* with f ranging from 500 kHz to 1 MHz to reduce measurement error from noise.

IV. Experimental Results

A. RGB Mini-LEDs

The *I-V* characteristics of mini-LED samples were tested with a source meter, as shown in Fig. 3(a), where the red LED uses the AlInGaP material, so the *I-V* curve shape is different from that of the other LEDs. The inset of Fig. 3(a) shows the normalized spectrum of the samples at a drive current of 2.00 mA. In

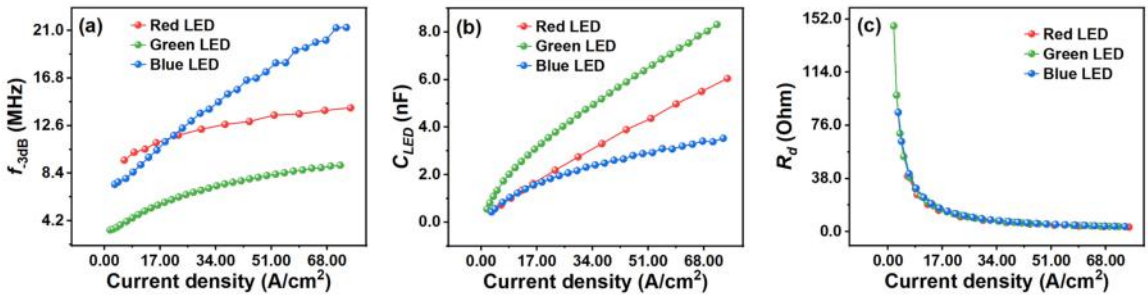

Fig. 5. (a) -3 dB cutoff frequency, (b) LED junction capacitance, and (c) differential resistance of RGB mini-LEDs.

addition, as shown in Fig. 3(b), the external quantum efficiency (EQE) curves of the LEDs were tested, where the maximum EQEs of RGB mini-LEDs correspond to current densities of approximately 50, 5, and 9 A/cm^2.

To investigate the differential carrier lifetime of RGB mini-LEDs and its dependence on the injected current, 12 mini-LEDs were tested, and the average error of the DLT was calculated, as shown in Fig. 4(a). The DLT of the LED decreases as the injected current density increases, which is in agreement with previous research [13], [24], [25]. At the same injected current density, the DLT of the blue mini-LED is significantly lower than that of the green mini-LED but not necessarily lower than that of the red mini-LED. The difference in DLT could be attributed to the different material and electrode structure of the RGB mini-LEDs. InGaN/GaN materials are commonly used for blue and green mini-LEDs, while AlInGaP materials are used for red mini-LEDs. Differences in DLT of LEDs made of different materials with the same chip size have been reported previously [7], [13], [25].The electrode structure of LEDs affects the injected current density [26], [27], and the DLT is closely related to the injected current density, as shown in Fig. 4, so the DLT could be affected by the LED electrode structure. A more in-depth study on the sources of DLT differences will be carried out in future work. Meanwhile, the DLT of the green mini-LED drops from 81.5 to 30.3 ns, whereas that of the blue mini-LED drops from 37.2 to 12.9 ns, which implies that the DLT of the green mini-LED drops faster than that of the blue mini-LED as the injected current density increases, consistent with previous results [13]. The DLT test results fluctuate very little at different injected current densities, with minimum and maximum mean errors of 2.81% and 22.64%, respectively, indicating good stability of the test method. Fig. 4(b) shows the full width at half maximum (FWHM) of the spectrum of the samples at various injected current densities. The FWHM values of the samples all gradually increase as the injected current density increases, which is attributed to the band filling effect of the LEDs [6], [28]. The DLT versus current relationship is opposite to the FWHM versus current relationship, as illustrated in Fig. 4.

The differential carrier lifetime for LEDs is approximately inversely proportional to the -3 dB cutoff frequency (f_{-3dB}), which can be expressed as follows [29]:

$$f_{-3\mathrm{dB}} = \frac{\sqrt{3}}{2\pi \times \mathrm{DLT}}. \tag{15}$$

LEDs in VLC systems have low-pass characteristics, and the higher the -3 dB cutoff frequency is, the greater the bandwidth [30]. As shown in Fig. 5(a), the -3 dB cutoff frequency increases as the injected current density increases, enhancing the bandwidth of the VLC systems from the LED perspective. However, determining the carrier lifetime of LEDs by testing the bandwidth of VLC systems introduces large errors because of the use of signal amplification, transmit-receive equalizers and impedance matching components in VLC systems to increase the bandwidth [31], [32].

When the LED is operating under forward bias, the LED junction capacitance is mainly influenced by the diffusion capacitance and the depletion layer capacitance [23]. The depletion layer capacitance is very small compared to the diffusion capacitance. Therefore, the depletion layer capacitance can be ignored when the LED is forward biased, and the LED junction capacitance (C_{LED}) can be approximately written as follows [33], [34], [35]:

$$C_{LED} = \frac{qI_{DC} \times \mathrm{DLT}}{2k_B T}, \tag{16}$$

where I_{DC} denotes the DC current, k_B denotes the Boltzmann constant, and T denotes the thermodynamic temperature. As shown in Fig. 5(b), the LED junction capacitance increases as the injected current density increases, and the junction capacitance of the green mini-LED rises significantly faster than that of the red and blue mini-LEDs. In addition, the RC time constant of the LED is approximately equal to the product of the differential resistance (R_d) and the LED junction capacitance (C_{LED}) and satisfies the following [17]:

$$R_d \approx \frac{\mathrm{DLT}}{C_{LED}}. \tag{17}$$

Fig. 5(c) reveals that R_d decreases as the injected current density increases and the reduction of R_d for the green mini-LED is larger than those for the red and blue mini-LEDs, which is attributed to the combined effect of C_{LED} and R_d, particularly the rapid change in R_d, according to Fig. 4(a). The study of junction capacitance and differential resistance of LEDs is one of the current research hotspots, especially for mini/micro-LEDs. The method proposed in this paper provides a gateway for the study of junction capacitance and differential resistance of

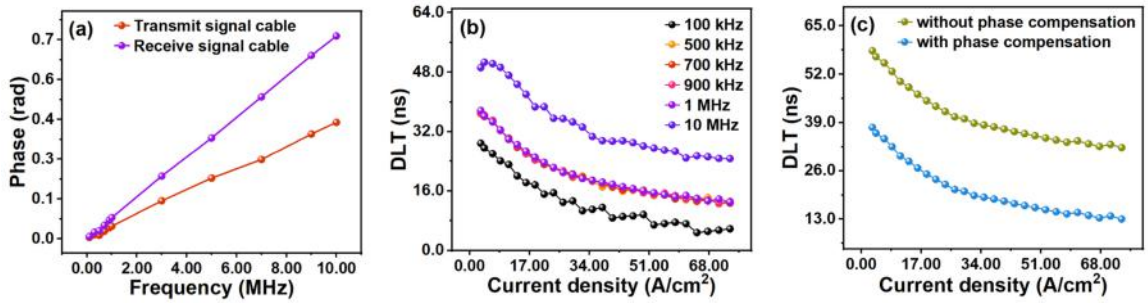

Fig. 6. (a) Phase delay of transmit and receive signal cables, (b) DLT of the blue mini-LED at different operating frequencies, and (c) DLT of the blue mini-LED before and after compensation of the phase delay from the cables.

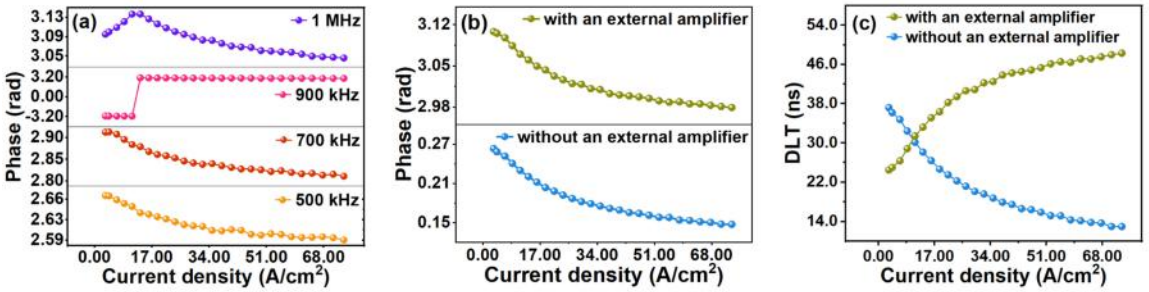

Fig. 7. (a) Phase difference θ when the measurement system has an external amplifier, (b) average phase difference for two cases, and (c) DLT with varied injected current density of the blue mini-LED at a controlled temperature of 300 *K*.

LEDs via (13), (16), and (17).

B. Measurement Error

The main measurement errors in the proposed measurement method and system originate from the cables and signal amplifier. The internal structure of the photodetector has parasitic parameters that affect the accuracy of the signal phase detection, but these are ignored in this paper because the effect of parasitic parameters in the photodetector is much smaller than that of cables and signal amplifiers. To reduce the measurement error, the same type of cable is used for both the transmit and receive signal cables in the system. Since the phase delay of the cables is different at various operating frequencies, using a fixed phase delay value to compensate for the delay caused by the cables is an inappropriate treatment.

As shown in Fig. 6(a), the phase delay of the transmit and receive signal cables was tested by the DSP lock-in amplifier. As the operating frequency increases, the phase delay from the cables becomes more severe. Moreover, according to the discussion on (14), as f increases, the AC amplitude of the light signal of the LED decreases, so it is not advisable to use high frequencies for system operation. In addition, when the LED operates at low frequencies, the phase difference is small, and the relative error of the system in the phase measurement increases. As shown in Fig. 6(b), with the blue mini-LED results as representative data, the DLT results fluctuate widely, and the test error increases when the system operates at 100 kHz and 10 MHz; however, the test results are stable in the range of 500 kHz to 1 MHz, which satisfies the frequency range recommended by the phase difference method for determining the differential carrier lifetime [13]. Therefore, the proposed method uses a frequency in the range of 500 kHz to 1 MHz, and multiple measurements are averaged to reduce the error. Fig. 6(c) shows the DLT results of the blue mini-LED before and after compensation of the phase delay from the cables. The results show that if the phase delay from the cables is not taken into account, then the test results will be much larger. According to the experimental results in Fig. 6(a), the DLT was measured based on (13) using the corresponding $\triangle\theta$ for different f, which is one of the advantages of the present method for error reduction.

The signal amplifier is one of the key components for carrier lifetime measurement using the phase difference method. Use of a signal amplifier (a type of discrete device), whether at the transmitter or receiver, will have a significant impact on the measurement results. The issue of discrete signal amplifiers adversely affecting the phase of a signal has been reported previously [13], [36], but not studied in detail. Discrete signal amplifiers have unknown parasitic parameters, especially parasitic inductance and capacitance, and the phase delay of the signal amplifier varies with the operating frequency and is difficult to predict and deduce in the test. An external signal amplifier is connected to the photodetector post-stage for comparative analysis to study the effect of the signal amplifier on the test results of the system. The suggested operating frequency of the proposed measurement system is between 500 kHz and 1 MHz, and in order to satisfy Nyquist's sampling theorem, the external signal amplifier bandwidth is at least 2 MHz, but since the photodetector bandwidth of the system is 1 GHz, the external signal amplifier with a bandwidth of 1 GHz is chosen in order to keep the bandwidth consistent in this work. The blue mini-LED data are used as representative data. To reduce the redundant data in this paper, and since blue and green mini-LEDs both use InGaN/GaN materials, the choice of the data of the blue mini-LED as a representative is without loss of generality. As shown in Fig. 7(a), the phase measurement results vary greatly with the change in frequency, and both phase lead and phase lag cases

TABLE I
COMPARISON OF EXISTING MEASUREMENT METHODS

Methods	Minimum Current (mA)	Property	Detection Technology	Discrete Signal Amplifier	Calibration	Accuracy	Cost
Ref. [6]	1	EL	Fitting the decay trace of an optical signal	NA	M	M	H
Ref. [7]	1	EL	Fitting the impedance of LEDs	Yes	D	NA	H
Ref. [10], [11]	5	EL	Measuring the -3 dB bandwidth of LEDs	NA	D	NA	H
Ref. [12]	NA	PL	Fitting the decay trace of an optical signal	No	D	NA	M
Ref. [13]	2	EL	Measuring the phase difference based on the rate equation	Yes	M	M	M
This work	0.1	EL	Measuring the phase difference based on the rate equation and phase-sensitive detection	No	G	H	M

Note: NA is short for "not available", EL is short for "electroluminescence"; PL is short for "photoluminescence"; "Yes" in the "Discrete Device" column indicates that a discrete signal amplifier was used in the test; G is short for "Good"; M is short for "Medium"; D is short for "Disabled"; the "Cost" column indicates the cost of the instrument; H is short for "High".

appear. Comparing before and after the external amplifier is added, the phase measurement results with the external amplifier are much larger than those without the external amplifier, as shown in Fig. 7(b). After compensation of the phase delay of the cables, the trend of DLT variation with the external amplifier is reverse to that without the external amplifier, leading to incorrect measurement results, as shown in Fig. 7(c). Therefore, it is not recommended to use discrete devices when using the phase difference method to measure the carrier lifetime because their parasitic parameters are unknown and difficult to predict, resulting in larger errors in the system during phase measurement, which affects the DLT results.

V. DISCUSSION AND CONCLUSION

The characteristics of the existing measurement methods were compared with those of this work, as summarized in Table I. The DLT detection principle was deduced in detail based on the rate equation and the phase-sensitive detection technique of the DSP lock-in amplifier. Our proposed measurement method demonstrates advantages in low-current scenarios and optimization of measurement errors. The measurement method and system proposed in this paper employ an integrated DSP lock-in amplifier to lock the optical signal to be measured and filter out high-frequency and noise signals, allowing for weak signal detection and support of scenarios with currents as low as 0.1 mA. Compared to previous methods, the proposed method has higher measurement accuracy and is less costly and complex than the TRPL method and the method of determining the carrier lifetime by measuring the LED bandwidth with a vector network analyzer. Carrier lifetime measurements for low-current scenarios guide the selection of the appropriate modulation depth and LED operating frequency for VLC systems. The test data for this method do not require a function approximation fitting operation based on the LED equivalent model. Because of the thermal and negative capacitance effects of LEDs operating at high currents [37], [38], [39], the relative error in determining the carrier lifetime by fitting the impedance of LEDs can be large, and the test data even cannot be fitted to the carrier lifetime. In addition, phase calibration of the transmit and receive signal cables was carried out innovatively, and no external discrete signal amplifiers were added to the measurement system, thus advantageously improving the stability of the measurement results and minimizing measurement errors.

The effect of the injected current density on the DLT of RGB mini-LEDs was investigated with the suggested method. As the injected current density increases, the DLT of the same LED decreases, and the DLT of green mini-LEDs decreases faster than that of blue mini-LEDs. The DLT decreases with increasing injected current density, whereas the FWHM increases with increasing injected current density. The method proposed in this paper also provides a way to study the junction capacitance and differential resistance of LEDs. The junction capacitance of the LED increases as the injected current density increases, while the differential resistance decreases. The measurement method employs a DSP lock-in amplifier to lock the light signal to be measured, filtering out high-frequency signals and noise and advantageously supporting DLT measurement in low-current scenarios. The transmit and receive signal cables are phase-calibrated before testing, and the system does not use discrete signal amplifiers, reducing measurement errors. The method proposed in this paper possesses significant advantages in terms of noise immunity, reduction of measurement error, adaptation to low-current scenarios, and cost reduction.

REFERENCES

[1] H. Haas, L. Yin, Y. Wang, and C. Chen, "What is LiFi?," *J. Lightwave Technol.*, vol. 34, no. 6, pp. 1533-1544, Mar. 2016, doi: 10.1109/JLT.2015.2510021.

[2] F. Yang, J. Wang, and Y. Dong, "Physical-Layer Security for Indoor VLC Wiretap Systems Under Multipath Reflections," *IEEE Trans. Wirel. Commun.*, vol. 21, no. 12, pp. 11179-11192, Dec. 2022, doi: 10.1109/TWC.2022.3190362.

[3] X. Cao, X. Wang, G. Chen, and X. Yang, "A Novel Visible Light Positioning System Based on the Dual-LED Anchor," *IEEE Trans. Instrum. Meas.*, vol. 72, pp. 1-12, 2023, Art no. 9506012, doi: 10.1109/TIM.2023.3259041.

[4] I. Cappelli et al., "Enhanced Visible Light Localization Based on Machine Learning and Optimized Fingerprinting in Wireless Sensor Networks," *IEEE Trans. Instrum. Meas.*, vol. 72, pp. 1-10, 2023, Art no. 9503410, doi: 10.1109/TIM.2023.3240220.

[5] T. Z. Gutema, H. Haas, and W. O. Popoola, "WDM Based 10.8 Gbps Visible Light Communication With Probabilistic Shaping," *J. Lightwave Technol.*, vol. 40, no. 15, pp. 5062-5069, Aug. 2022, doi: 10.1109/JLT.2022.3175575.

[6] JIH. Haggar, SS. Ghataora, V. Trinito, J. Bai, and T. Wang, "Study of the Luminescence Decay of a Semipolar Green Light-Emitting Diode for Visible Light Communications by Time-Resolved Electroluminescence," *ACS Photonics*, vol. 9, no. 7, pp. 2378-2384, Jul. 2022, doi: 10.1021/acsphotonics.2c00414.

[7] A. Rashidi, M. Monavarian, A. Aragon, A. Rishinaramangalam, and D. Feezell, "Nonpolar *m*-Plane InGaN/GaN Micro-Scale Light-Emitting

Diode With 1.5 GHz Modulation Bandwidth," *IEEE Electron Device Lett*., vol. 39, no. 4, pp. 520-523, Apr. 2018, doi: 10.1109/LED.2018.2803082.

[8] J. Kowal, D. Hente, and D. U. Sauer, "Model Parameterization of Nonlinear Devices Using Impedance Spectroscopy," *IEEE Trans. Instrum. Meas.*, vol. 58, no. 7, pp. 2343-2350, Jul. 2009, doi: 10.1109/TIM.2009.2013927.

[9] A. Rashidi, et al., "Differential carrier lifetime and transport effects in electrically injected III-nitride light-emitting diodes," *J. Appl. Phys.*, vol. 122, no. 3, Jul. 2017, doi: 10.1063/1.4994648.

[10]P. -G. Eliseev, M. Osin'ski, and H. Li, "Recombination Balance in Green-light-emitting GaN/InGaN/AlGaN Quantum Wells," *Appl. Phys. Lett.*, vol. 75, no. 24, pp. 3838-3840, Dec. 1999, doi: 10.1063/1.125473.

[11]R. P. Green, J. J. D. McKendry, D. Massoubre, E. Gu, M. D. Dawson, and A. E. Kelly, "Modulation Bandwidth Studies of Recombination Processes in Blue and Green InGaN Quantum Well Micro-light-emitting diodes," *Appl. Phys. Lett.*, vol. 102, no. 9, pp. 1-4 Mar. 2013, doi: 10.1063/1.4794078.

[12]I. Reklaitis, et al., "Differential Carrier Lifetime in InGaN-based Light-emitting Diodes Obtained by Small-signal Frequency-domain Measurements," *J. Appl. Phys.*, vol. 121, no. 3, pp. 1-6, Jan. 2017, doi: 10.1063/1.4973903.

[13]X. Meng, et al., "Study on Efficiency Droop in InGaN/GaN Light-emitting Diodes Based on Differential Carrier Lifetime Analysis," *Appl. Phys. Lett.*, vol. 108, no. 1, pp. 1-4, Jan. 2016, doi: 10.1063/1.4939593.

[14]X. Deng, K. Arulandu, Y. Wu, G. Zhou, and J. -P. M. G. Linnartz, "Performance Analysis for Joint Illumination and Visible Light Communication Using Buck Driver," *IEEE Trans. Commun.*, vol. 66, no. 5, pp. 2065-2078, May. 2018, doi: 10.1109/TCOMM.2018.2792018.

[15]L. Wang, X. Wang, J. Kang and C. P. Yue, "A 75-Mb/s RGB PAM-4 Visible Light Communication Transceiver System With Pre- and Post-Equalization," *J. Lightwave Technol.*, vol. 39, no. 5, pp. 1381-1390, 1 Mar. 2021, doi: 10.1109/JLT.2020.3034227.

[16]Agrawal, G. P, "Fiber-optic Contiminications Systems," 4th ed, John Wiley and Sons, New York, 2010, pp. 113-121.

[17]Z. Wei, et al., "Parallel Mini/Micro-LEDs Transmitter: Size-Dependent Effect and Gbps Multi-User Visible Light Communication," *J. Lightwave Technol.*, vol. 40, no. 8, pp. 2329-2340, Apr. 2022, doi: 10.1109/JLT.2021.3138626.

[18]A. David and M. J. Grundmann, "Droop in InGaN Light-emitting Diodes: A Differential Carrier Lifetime Analysis," *Appl. Phys. Lett.*, vol. 96, no. 10, pp. 1-3, Mar. 2010, doi: 10.1063/1.3330870.

[19]L. Riuttanen, et al., "Recombination Lifetime in InGaN/GaN Based Light Emitting Diodes at Low Current Densities by Differential Carrier Lifetime Analysis," *Phys. Status Solidi C*, vol. 10, no. 3, pp. 327-331, Jan. 2013, doi: 10.1002/pssc.201200670.

[20]Z. Wang, X. Shi, W. Wang, and W. Cai, "High-Performance Digital Lock-In Amplifier Module Based on an Open-Source Red Pitaya Platform: Implementation and Applications," *IEEE Trans. Instrum. Meas.*, vol. 72, pp. 1-14, Mar. 2023, doi: 10.1109/TIM.2022.3221746.

[21]M. P. Halsall, I. F. Crowe, J. Mullins, R. A. Oliver, M. J. Kappers, and C. J. Humphreys, "Photomodulated Reflectivity Measurement of Free-Carrier Dynamics in InGaN/GaN Quantum Wells," *ACS Photonics*, vol. 5, no. 11, pp. 4437–4446, Oct. 2018, doi: 10.1021/acsphotonics.8b00904.

[22]I. Reklaitis, et al., "Time of Carrier Escape and Recombination Coefficients in InGaN Quantum-well Active Regions of Blue, Cyan, and Green Light-emitting Diodes," *Semicond. Sci. Technol.*, vol. 34, no. 1, pp. 1-11, Jan. 2019, doi: 10.1088/1361-6641/aaef06.

[23]Y. Huang, Z. Guo, X. Wang, H. Li, and D. Xiang, "GaN-Based High-Response Frequency and High-Optical Power Matrix Micro-LED for Visible Light Communication," *IEEE Electron Device Lett.*, vol. 41, no. 10, pp. 1536-1539, Oct. 2020, doi: 10.1109/LED.2020.3021282.

[24]H. Xiao, K. Wang, R. Wang, W. Chen, and K. S. Chiang, "Equivalent Circuit of Quantum-Dot LED and Acquisition of Carrier Lifetime in Active Layer," *IEEE Electron Device Lett*., vol. 41, no. 1, pp. 87-90, Jan. 2020, doi: 10.1109/LED.2019.2954326.

[25]M. Monavarian, et al., "Explanation of Low Efficiency Droop in Semipolar (2021) InGaN/GaN LEDs through Evaluation of Carrier Recombination Coefficients," *Opt. Express*, vol. 25, no. 16, pp. 19343-19353, Aug. 2017, doi: 10.1364/OE.25.019343.

[26]X. Zheng, et al., "Enhanced Light Output Power from AlGaN-based Deep Ultraviolet LEDs Achieved by a Four-in-one Mesa Structure," *Appl. Phys. Lett.*, vol. 123, no. 1, pp. 1-8, Jul. 2023, doi: 10.1063/10.1063/5.0157081.

[27]F. Olivier, A. Daami, C. Licitra, and F. Templier, "Shockley-Read-Hall and Auger Non-radiative Recombination in GaN Based LEDs: A Size Effect Study," *Appl. Phys. Lett.*, vol. 111, no. 1, pp. 1-5, Jul. 2017, doi: 10.1063/10.1063/1.4993741.

[28]J. Zhao, et al., "GaN-based Parallel Micro-light-emitting Diode Arrays with Dual-Wavelength InxGa1-xN/GaN MQWs for Visible Light Communication," *Opt. Express*, vol. 30, no. 11, pp. 18461-18470, May. 2022, doi: 10.1364/OE.452679.

[29] I. V. Frolov, V. A. Sergeev, and O. A. Radaev, "The Method for Measuring the Distribution Profile of the 3-dB Frequencies of Electroluminescence Over the Area of the LED Chip," *IEEE Trans. Instrum. Meas.*, vol. 72, pp. 1-6, 2023, Art no. 5000806, doi: 10.1109/TIM.2022.3206812.

[30]X. Deng, et al., "Mitigating LED Nonlinearity to Enhance Visible Light Communications," *IEEE Trans. Commun.*, vol. 66, no. 11, pp. 5593-5607, Nov. 2018, doi: 10.1109/TCOMM.2018.2858239.

[31]L. Teixeira, et al., "A Review of Visible Light Communication LED Drivers," *IEEE J. Emerg. Sel. Top. Power Electron.*, vol. 10, no. 1, pp. 919-933, Feb. 2022, doi: 10.1109/JESTPE.2021.3092284.

[32]Z. -Y. Wu, Y. -L. Gao, J. -S. Wang, X. -Y. Liu, and J. Wang, "A Linear Current Driver for Efficient Illuminations and Visible Light Communications," *J. Lightwave Technol.*, vol. 36, no. 18, pp. 3959-3969, Sep. 2018, doi: 10.1109/JLT.2018.2854914.

[33]Y. Huang, Z. Guo, H. Huang, and H. Sun, "Influence of Current Density and Capacitance on the Bandwidth of VLC LED," *IEEE Photonics Technol. Lett.*, vol. 30, no. 9, pp. 773-776, May, 2018, doi: 10.1109/LPT.2018.2813665.

[34]L. Guo, Y. Guo, J. Yang, J. Yan, J. Liu, J. Wang, and T. Wei, "275 nm Deep Ultraviolet AlGaN-Based Micro-LED Arrays for Ultraviolet Communication," *IEEE Photonics J.*, vol. 14, no. 1, pp. 1-5, Feb. 2022, Art no. 8202905, doi: 10.1109/JPHOT.2021.3129648.

[35]M. L. Lucia, J. L. Hernandez-Rojas, C. Leon, and I. Martil, "Capacitance Measurements of p-n Junctions: Depletion Layer and Diffusion Capacitance Contributions, " *Eur. J. Phys.*, vol. 14, pp. 86–89, Jan. 1999, doi: 10.1088/0143-0807/14/2/009.

[36]S. Watson, H. C. Wee, H. Griffiths, and R. J. Williams, "A Highly Phase-stable Differential Detector Amplifier for Magnetic Induction Tomography," *Physiol. Meas.*, vol. 32, no. 7, pp. 917-926, Jul. 2011, doi: 1010.1088/0967-3334/32/7/S14.

[37]Y. Liu, K. Zhang, B.-R. Hyun, H. S. Kwok, and Z. Liu, "High-brightness InGaN/GaN micro-LEDs with secondary peak effect for displays," *IEEE Electron Device Lett.*, vol. 41, no. 9, pp. 1380–1383, Sep. 2020, doi:10.1109/LED.2020.3014435.

[38]C.-L. Liao, C.-L. Ho, Y. -F. Chang, C.-H. Wu, and M.-C. Wu, "High-speed light-emitting diodes emitting at 500 nm with 463-MHz modulation bandwidth," *IEEE Electron Device Lett.*, vol. 35, no. 5, pp. 563–565, May. 2014, doi: 10.1109/LED.2014.2304513.

[39]D. -P. Han, Y. -J. Kim, J. -I. Shim, and D. -S. Shin, "Forward-Capacitance Measurement on Wide-Bandgap Light-Emitting Diodes," *IEEE Photonics Technol. Lett.*, vol. 28, no. 21, pp. 2407-2410, Nov. 2016, doi: 10.1109/LPT.2016.2597158.

Chen-Ming Zhong (Graduate Student Member, IEEE) received the M.S. degree from School of Information Engineering, Nanchang University, Nanchang, China, in 2015.

He is currently pursuing the Ph.D. degree at the Department of Electronic Science, Xiamen University, Xiamen, China. His research interests focus on semiconductor lighting and testing.

Jing-Yu Deng received the B.S. degree in Applied Physics from the China University of Mining and Technology, Xuzhou, China, in 2021.

She is currently pursuing the M.S. degree in physical electronics at Xiamen University, Xiamen, China. Her current research interests are semiconductor lighting and inspection.

Xi Zheng received the B.S. degree from College of Physics, Jilin University, Changchun, China, in 2019.

He is currently pursuing the Ph.D. degree at the Department of Electronic Science, Xiamen University, Xiamen, China. His research interests focus on the development and characterization of high efficiency micro-LEDs.

Chang-Dong Tong received the M.S. degree from the School of Electronic Science and Engineering, Xiamen University, Xiamen, China, in 2022, where he is currently pursuing the Ph.D. degree.

His research interests include miniature light emitting diode (LED) devices application.

Guo-Bao Zhao received the M.S. degree from the School of Automation, Harbin Institute of Technology, Harbin, China, in 2020. He is currently pursuing the Ph.D. degree at the Department of Electronic Science, Xiamen University, Xiamen, China.

His research interests include Solid-state lighting testing and applications, hyperspectral instrument development, and machine learning.

Guo-Long Chen received the M.S. degree from Xiamen University, Xiamen, China, in 1998.

He has been a Senior Experimenter with the Department of Electronic Science, Xiamen University. His research interests focus on semiconductor lighting inspection technology and application.

Hui-Hui Meng received the B.S. degree from Sun Yat-sen University, Guangzhou, China, in 2017.

He has been a senior engineer with Guangzhou Sine Scientific Instrument Co., Ltd. His research interests focus on weak signal detection technology development and application.

Li-Hong Zhu received the Ph.D. degree in microelectronics and solid-state electronics from Xiamen University, Xiamen, China, in 2010.

Since 2013, she has been a Senior Engineer with the Department of Electronic Science, Xiamen University. Her research interests include the III-nitride based light-emitting diode materials and devices.

Yi-Jun Lu received the Ph.D. degree in condensed matter physics from Xiamen University, Xiamen, China, in 2000.

He was with the Department of Physics, Xiamen University, till 2011. Since then, he has been with the Department of Electronic Science, Xiamen University, where he is currently a Professor. His research interests focus on Solid-state lighting testing and application.

Zhong Chen received the Ph.D. degree from Xiamen University, Xiamen, China, in 1993.

Since 2000, he has been a Professor with the Department of Physics and Department of Electronic Science, Xiamen University, respectively. His research interests focus on scientific instrument design and nuclear magnetic resonance.

Wei-Jie Guo (Member, IEEE) received the Ph.D. degree in physical electronics from Xiamen University, Xiamen, China, in 2019.

Since 2020, he has been an Assistant Professor with the Department of Electronic Science, Xiamen University. His research interests include the III-nitride-based devices and light-emitting diode displays.